Title	Three-dimensional static speckle fields. Part II. Experimental investigation
Authors(s)	Li, Dayan; Kelly, Damien P.; Sheridan, John T.
Publication date	2011-09-01
Publication information	Journal of the Optical Society of America A, 28 (9): 1904-1908
Publisher	Optical Society of America
Link to online version	http://dx.doi.org/10.1364/JOSAA.28.001904
Item record/more information	http://hdl.handle.net/10197/3298
Publisher's statement	This paper was published in Journal of the Optical Society of America. A, Optics and image science and is made available as an electronic reprint with the permission of OSA. The paper can be found at the following URL on the OSA website: http://www.opticsinfobase.org/josaa/abstract.cfm?uri=josaa-28-9-1904. Systematic or multiple reproduction or distribution to multiple locations via electronic or other means is prohibited and is subject to penalties under law.
Publisher's version (DOI)	10.1364/JOSAA.28.001904

Three-dimensional static speckle fields. Part II. Experimental investigation

Dayan Li,[1] Damien P. Kelly,[2] and John T. Sheridan[1,*]

[1]*UCD Communications and Optoelectronic Research Centre, SFI-Strategic Research Cluster in Solar Energy Conversion, School of Electrical, Electronic and Mechanical Engineering, College of Engineering, Mathematical and Physical Sciences, University College Dublin, Belfield, Dublin 4, Ireland*

[2]*Institut für Mikro- und Nanotechnologien, Macro-Nano, Fachgebiet Optik Design, Technische Universität Ilmenau, Postfach 100565, 98684 Ilmenau, Germany*

**Corresponding author: john.sheridan@ucd.ie*

Received June 15, 2011; accepted July 12, 2011;
posted July 25, 2011 (Doc. ID 149204); published August 25, 2011

In Part I [J. Opt. Soc. Am. A **28**, 1896 (2011) of this paper, the physical model for fully developed speckle is examined based on two critical assumptions. (i) It is assumed that in the object plane, the speckle field is delta correlated, and (ii) it is assumed that the speckle field in the observation plane can be described as a Gaussian random process. A satisfactory simulation technique, based on the assumption that spatial averaging can be used to replace ensemble averaging, is also presented. In this part a detailed experimental investigation of the three-dimensional speckle properties is performed using spatial averaging. The results provide solid verification for the predictions presented in Part I. The results are not only of theoretical interest but have practical implications. Techniques for locating and aligning the optical system axis with the camera center, and for measuring out-of-plane displacement, are demonstrated.

OCIS codes: 030.6140, 030.6600, 050.1940, 070.7345, 200.2610.

1. INTRODUCTION

In Part I [1], based on the physical model for fully developed speckle, we reviewed the derivation of the three-dimensional (3D) correlation function $|\mu_{12}|^2$ [2–4]. Applying $|\mu_{12}|^2$, the lateral and longitudinal speckle decorrelation characteristics, and thus speckle size, are examined using both analytic expressions and numerical simulations. Significantly, however, as noted in [5,6], the longitudinal and off-axis properties of speckle fields have rarely been experimentally examined. Furthermore, the existing experimental studies have not produced consistent results [7,8]. Recently, the longitudinal speckle size has been experimentally examined for Fresnel propagation and single lens linear canonical transform optical system cases, (see [9] and Chapter 8 in [10]). However, in [9,10] the theoretical expressions for the off-axis longitudinal speckle sizes are not consistent with the more physically accurate expression for $|\mu_{12}|^2$, presented in Part I [1]. In Part II of this paper, the results of a detailed series of experiments are presented and compared to the analytic predictions presented in Part I [1]. It is shown that the experimental results provide consistent verification of the commonly applied physical model (assuming Delta correlated field in the object plane). Therefore, a practical means to investigate the 3D speckle properties and the implied applications has been presented.

This paper is organized as follows. In Section 2 we begin by describing the experiment arrangement used to measure the speckle correlation coefficients. To achieve high measurement accuracy, it was found necessary to center the camera with respect to the optical axis (principal axis of the optical system). In Subsection 2.A it is shown how this can be achieved, by applying the statistical properties of the speckle field discussed in Part I. In Subsection 2.B both the lateral and longitudinal correlation coefficients predicted by the physical model are measured and shown to agree well with the predictions (and numerical simulations) presented in Part I. Some experimental results to measure the out-of-plane displacement of the diffuser using off-axis speckle patterns are also provided. In Section 3, we present some concluding remarks.

Before proceeding, we recall that in Part I it was found that the theoretical predictions regarding the speckle characteristics for plane wave and Gaussian beam illumination were very similar. They only differ significantly in their predicted on-axis longitudinal decorrelation rates and the associated on-axis longitudinal speckle size. We note that the simulation algorithm, discussed in Part I, confirms this prediction. Therefore, in this paper only experimental results for the Gaussian beam illumination case are presented, clearly however our conclusions will also in general be applicable to the plane wave case.

2. EXPERIMENT

In order to perform accurate quantitative speckle correlation, it is important to know the position of the subset image center with respect to the optical axis. In this section we first locate and center the optical axis with the camera using the observed decorrelation property of speckle along the radial direction (see Part I, Fig. 5 [1]). We then perform experiments to measure the lateral and longitudinal decorrelation trends. Results demonstrating the measurement of the out-of-plane displacement of the ground glass diffuser, in agreement with the predictions of Eq. (12) in Part I [1], are also provided.

The experimental system used is shown in Fig. 1. A Gaussian beam from a helium–neon laser of wavelength $\lambda = 633\,\text{nm}$ is spatially filtered and then collimated by a lens of focal length $f = 10\,\text{cm}$. An optical diffuser (100 mm diameter

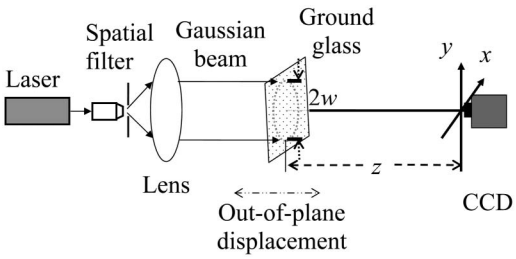

Fig. 1. Optical arrangement for the static speckle formation in the Fresnel regime under illumination of a Gaussian beam.

120 Grit Ground Glass Diffuser) is used, and the illuminating spot on this object is measured to have a diameter of $2w = 8.8$ mm. The speckle image is recorded using a CCD camera positioned as shown in the observation plane that is perpendicular to the optical axis. The CCD is mounted on a translation stage, which can move in both the x and y directions, so that the position of the CCD center can be adjusted (this will be discussed in relation to the alignment algorithm in Subsection 2.A). The ground glass diffuser is mounted on a separate translation stage in the object plane, which can be used to produce accurate out-of-plane displacements as shown. The CCD used is an 8 bit 4 megapxiel IMPERX IPX-4M15-G, which has 2048×2048 pixels each of size $7.4\,\mu$m. The translation stages used (NewPort UTS50PP linear stage) have a positional accuracy of $\pm 0.1\,\mu$m.

Please note that in the theoretical derivation and the numerical simulation presented in Part I [1], the longitudinal displacement of the speckle fields is achieved in the observation plane. This is different from the experimental setup we present here where longitudinal displacement takes place in the object plane by longitudinally moving the diffuser. Whether the longitudinal displacement is generated in the object plane or in the observation plane, unwanted relative in-plane displacement or tilt of the diffuser and the camera should be avoided because the correlation function presented in [1] has not included such effects. If only longitudinal displacement takes place, it is obvious that the two methods are equivalent for the free-space Fresnel geometry we are examining in this paper. We use this setup mainly with the aim of demonstrating the potential application of speckle correlation property on out-of-plane displacement measurements, as indicated by the experimental results shown in Table 1. However, during the experiment, if in-plane displacement or tilt of the diffuser takes place, the illuminated area on the diffuser surface before and after the longitudinal displacement would be different. This will reduce the correlation between the two patterns as the statistics of the microstructures that generate the speckle patterns might differ much with each other. Using an experimental setup where longitudinal displacement is generated in the observation plane, this problem does not arise. Fortunately, the in-plane displacement or tilt of the diffuser arising in our experiment is relatively easy to reduce to negligible levels by normal experimental skills, e.g., using a collimated illuminating beam and carefully adjusting the longitudinal displacement direction. In order to model the case when in-plane displacement or tilt becomes significant, Eq. (12) in Part I must be modified before being applied to measure the out-of-plane displacement, as in this case the theoretical correlation function is different from those presented in Part I. For further insights into the influence of the in-plane displacement and tilt of the diffuser on the correlation function, readers are referred to [11–14].

A. Locating and Centering the Optical Axis

Two longitudinally displaced speckle patterns in the observation plane are used to locate and center the optical axis with respect to the camera. The two captured speckle pattern images are both divided into smaller subimages, see Fig. 2. Each subimage pair is made up of a subimage from $z = z_0$ and a subimage from $z = z_0 + \varepsilon$, with the two subimages being located opposite of one another, i.e., at the same distances from their respective image centers. Correlation calculations are then carried out for each subimage pair.

Based on the results, the following two phenomena are observed: (i) the longitudinal correlation coefficient values between each subimage pair is different; however, the largest value is always produced by the subimage pair which is most closely aligned with the optical axis of the system. (ii) The longitudinal correlation coefficients decrease monotonically with increased radial displacement of the subimage pairs from the optical axis.

In Fig. 2, the image captured by the camera is divided into an odd number of subimages (here 5×5). The optical axis is

Table 1. Out-of-Plane Displacement Measurement Results

	z_0 (mm)	ε (μm)	x (mm)	Maximum Correlation	Measured γ (subpixel)	Measured ε (μm)	Discrepancy
1	80	100	2.22	0.6373	0.2523	67.22	32.78%
2			4.44	0.695	0.8333	111.08	11.08%
3			6.66	0.7809	1.0263	91.26	8.74%
4	250	100	2.22	0.9818	0.1019	84.49	15.51%
5			4.44	0.9663	0.2010	83.75	16.25%
6			6.66	0.9384	0.3255	90.41	9.59%
7	250	500	2.22	0.8026	0.5907	492.26	1.55%
8			4.44	0.8383	1.1365	473.54	5.29%
9			6.66	0.8292	1.7725	492.36	1.53%
10	250	1000	2.22	0.6079	1.2227	1018.94	1.89%
11			4.44	0.5918	2.3306	971.06	2.89%
12			6.66	0.5742	3.5597	988.83	1.12%
13	250	100	20.00	0.9817	1.0423	94.41	5.59%
14		500	20.00	0.8174	5.3280	492.84	1.43%
15		1000	20.00	0.6028	10.6913	988.95	1.11%

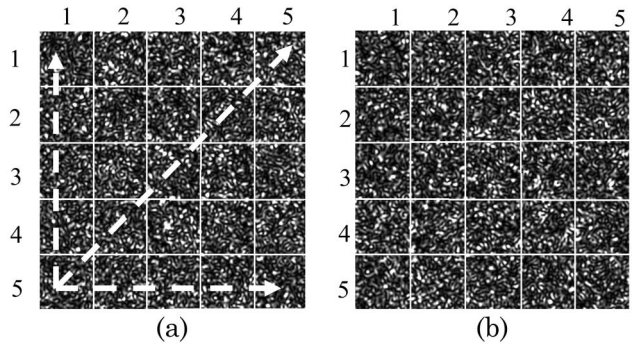

Fig. 2. Illustration of two longitudinally displaced speckle pattern images: (a) at $z = z_0$ and (b) $z = z_0 + \varepsilon$. Each has been divided into 25 subimages in order to observe the longitudinal correlation coefficients variations along the radial directions.

initially located in the region of the corner subimage pair, whose location is identified by the coordinates (5, 5). The three dashed white arrows appearing in Fig. 2(a) indicate radial directions along which the correlation coefficients decrease monotonically. As a result, centering of the optical axis is achieved using the following algorithm.

Step 1: identify the location of the optical axis and center the camera.

Identify the subimage pair having the maximum coefficient. The camera is then translated in-plane in the horizontal and vertical directions. New speckle images are captured and processed until the maximum value is identified occurring at the centrally located subimage pair, (3, 3), in Fig. 2. Step 1 is repeated until the camera is centered.

Step 2: decrease the size of the subimages in order to achieve more accurate centering.

We have found that better centering can be typically achieved by further subdividing the central image area(s) into an odd number of subimages and repeating Step 1.

As might be expected, this algorithm cannot be applied with ever increasing accuracy. A test or threshold value must be identified beyond which no further improvements in accuracy takes place. For example, Step 2 should stop once the monotonic property of the correlation along the radial direction is no longer unambiguously observed. Specifically, we note that the further the subimage pair is away from the optical axis, the lower the correlation coefficient value that should be found. When the threshold of accuracy is reached, the location of the maximum correlation coefficient no longer changes consistently during the offset correcting process. This breakdown has been identified as arising for two main reasons: First, the longitudinal correlation coefficients become less sensitive to radial offset as the subimage pairs are closer to the optical axis. For example, examining Fig. 5 in Part I [1], we see that the slope of the correlation curve is almost zero (it is flat) for small r. Second, the size of speckle image, i.e., the number of pixels in each subimage, should not be so small that the spatial average can well approximate the ensemble average. A sufficiently large subimage size is necessary to guarantee that the speckle field can be assumed ergodic and stationary in space.

Experimental results produced by applying Step 1 and Step 2 are provided in Figs. 3(a) and 3(b), respectively. The parameter values used are $z_0 = 250\,\text{mm}$, $\varepsilon = 0.5\,\text{mm}$, and $w = 4.4\,\text{mm}$. Figure 3(a) shows the central image area of 2045×2045 pixels

	1	2	3	4	5
1	0.135	0.252	0.337	0.289	0.154
2	0.240	0.479	0.642	0.558	0.313
3	0.312	0.616	0.821	0.699	0.388
4	0.275	0.519	0.678	0.566	0.305
5	0.155	0.290	0.371	0.302	0.161

(a)

	1	2	3	4	5
1	0.696	0.757	0.783	0.773	0.736
2	0.756	0.810	0.839	0.819	0.788
3	0.774	0.834	0.854	0.848	0.802
4	0.765	0.817	0.845	0.839	0.799
5	0.728	0.775	0.806	0.795	0.750

(b)

Fig. 3. (Color online) Experimental results of the longitudinal correlation coefficients for the subimage pairs. (a) Results for Step 1, the central active area of the camera is divided into 25 subimages, each subimage has 409×409 pixels. (b) Final results for Step 2, the central image region of size 605×605 is divided into 25 subimages, each subimage has 121×121 pixels.

divided into 5×5 subimages. The maximum correlation coefficient is located in subimage (3, 3), and the monotonically decreasing property, along the radial directions, is clearly observable, indicating that the optical axis is indeed located somewhere in this central 409×409 pixel region. As we can see in Fig. 3(a), the correlation coefficients in the lower right region $\{(4,4),(5,5),(1,2),\text{and}\,(2,1)\}$ are larger than their counterparts in the higher left region $\{(2,2),(1,1),(5,4)\,\text{and}\,(4,5)\}$, which indicates that the optical axis is actually located in the lower right area of subimage (3, 3). Since the size of the subimage at this point is still large, Step 2 can be applied. Figure 3(b) represents the final centering operation possible before the threshold behavior discussed above is reached. Figure 3(b) contains the results found using the central image of size 605×605 pixels that has been divided into 5×5 subimages. Following the same analysis described for Fig. 3(a), the location of the optical axis can be identified situating in the lower right region of subimage (3, 3). Since we consider the center of the subimage to be the location where the optical axis passes through the CCD, the achievable resolution of the centering process is approximately equal to half the number of pixels in the final subimage, that is $(605/5/2) \times 7.4\,\mu\text{m}$, implying an accuracy of $\pm 447.7\,\mu\text{m}$ in r.

Importantly, however, we wish to emphasis that these results based on repeated experimental measurements provide clear quantitative verification of the decorrelation properties described in Fig. 5 in Part I [1].

B. Experimental Results for Speckle Decorrelation

Having identified and positioned the optical axis at the center of the CCD, speckle pattern images can be captured to measure the general decorrelation trends predicted in Part I [1]. To study the lateral decorrelation trends, three speckle patterns are captured in the $z = z_0 + \varepsilon$ plane ($z_0 = 250\,\text{mm}$ and $\varepsilon = 0$, 0.5, and 1 mm). Subset images of size 200×200 pixels are selected from these patterns and correlated using the discrete correlation algorithm, the same as that used to perform the numerical simulation presented in Part I. The SOP [1,4] for these subset images is $\{Q_1 = (x_1, 0) = (4.44\,\text{mm}, 0)\}$. The results are shown in Fig. 4, where γ is given in terms of a number of pixels.

In order to compare the experimental results to the analytic continuous correlation function [Eq. (11) in Part I [1]], the discrete correlation coefficients obtained at each pixel position are interpolated. Figure 4 is generated using a cubic spline interpolation algorithm [15]. As can be seen, the interpolated experimental curves match the theoretical predictions reasonably well.

For the longitudinal decorrelation trends, ten speckle patterns are captured at $z = z_0 + \varepsilon$ ($z_0 = 250\,\text{mm}$ and $0 \le \varepsilon \le 1.8\,\text{mm}$, in steps of 0.2 mm). Correlation coefficients for four standard observation positions (SOPs), i.e., $Q = (x, 0) = \{(0, 0), (2.22\,\text{mm}, 0), (4.44\,\text{mm}, 0),$ and $(6.66\,\text{mm}, 0)\}$, were measured, so that the behavior of both on-axis and off-axis longitudinal correlation coefficients could be examined and compared with the analytic predictions. The results are shown in Fig. 5.

The out-of-plane displacement of the diffuser can be estimated in the observation plane using the experimental arrangement. Equation (12) in Part I [1] indicates that the measured value of the out-of-plane displacement is determined by several parameters, including the recording distance z_0, the off-axis observation position x (with respect to the optical axis), and the measured shift γ of the peak correlation coefficient. In order to improve the measurement accuracy for a given optical system, it is necessary to achieve subpixel

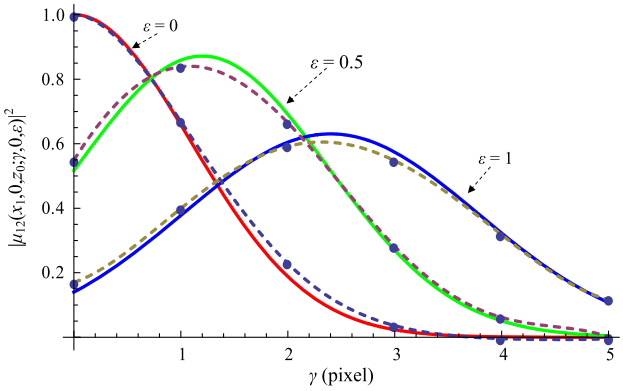

Fig. 4. (Color online) Lateral speckle correlation function for an off-axis field at $Q_1 = (x_1, 0)$ versus lateral shifting γ when $\varepsilon = 0\,\text{mm}$, $\varepsilon = 0.5\,\text{mm}$, $\varepsilon = 1\,\text{mm}$. Dots: discrete correlation coefficients from the experiment. Dashed curve: cubic spline interpolation based on the experimental data. Solid curve: theoretical continuous speckle correlation.

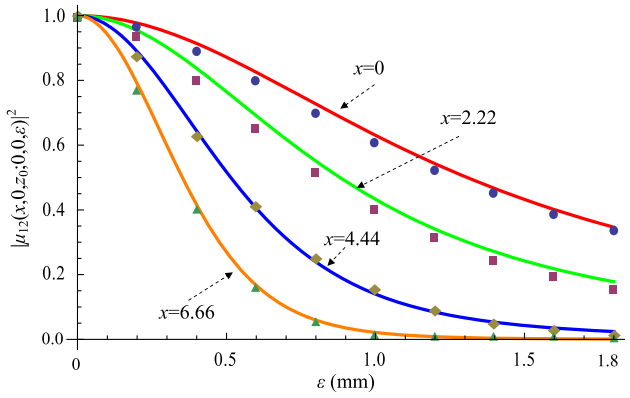

Fig. 5. (Color online) Longitudinal speckle correlation function for an off-axis field at $Q = (x, 0)$ versus longitudinal displacement ε when $x = 0\,\text{mm}$ (on-axis), $x = 2.22\,\text{mm}$, $x = 4.44\,\text{mm}$, and $x = 6.66\,\text{mm}$. Dots: discrete correlation coefficients from the experiment. Solid curve: theoretical continuous speckle correlation.

estimation for the extracted value of γ. This can be done using the method employed to generate Fig. 4 by interpolating the discrete coefficients to approximate a continuous correlation function. In this way, the position of the peak correlation γ is determined with subpixel accuracy.

To qualitatively examine the impact of these three parameters (z_0, x, and γ) on an out-of-plane displacement measurement, various experimental system values are chosen for the purpose of comparison, see Table 1. The effects of using different parameter values are compared: for z_0 (compare Rows 1–3 with Rows 4–6), for x (compare Rows 7–9 or Rows 10–12), and for the maximum correlation between the speckle patterns before and after the displacement (compare Rows 4–6, with Rows 7–9, and Rows 10–12). Finally the measured results, achieved using the optimized parameter values, are presented in Rows 13–15.

Examining the results presented in Table 1, we can conclude that the recording distance z_0 primarily affects the maximum correlation coefficient between the two speckle patterns before and after displacement. It is easy to prove, using the analytic equations, i.e., Eq. (9) or Eq. (11) in Part I [1], that for fixed values of w and ε the higher the maximum correlation is, the wider the lateral correlation curve becomes. A wider curve is usually accompanied by larger uncertainty in the estimation of γ, which results in a larger difference between the measured displacement and the actual true value. On the other hand, it is clear from Table 1 that x is the most influential parameter of the three examined. Generally, the larger the value of x, the more accurate the estimated displacement value will be. In Table 1 (Row 13–15), the results are provided for the case when $x = 20\,\text{mm}$ for various displacement $\varepsilon = 0.1$, 0.5, and 1 mm. In this case, the measurement error is approximately one pixel pitch of the camera (7.4 μm).

Further work is needed to more fully determine the ultimate achievable accuracy using this technique. However, the quantitative relationship between the parameters appearing in Eq. (12), in Part I [1] has been experimentally verified.

3. CONCLUSIONS

The physical model used to describe the statistical properties of fully developed static speckle in free space has been

verified experimentally by accurately measuring the correlation coefficients in 3D. The analytic space cross-correlation function of speckle has predicted two important properties.

i. The longitudinal correlation coefficients of two longitudinally displaced speckle patterns decrease monotonically along the radial direction away from the system optical axis, and

ii. position shifting of the peak coefficient is observed when an off-axis speckle pattern is correlated with the fields from a longitudinally displaced plane.

It has been shown, based on property (i), that the location of the optical axis with respect to the camera center can be accurately located. Such centering of the camera greatly improves the accuracy of both lateral and longitudinal speckle correlation coefficients measurement. It has also been shown, in relation to property (ii), that a quantitative relationship between the shifted value and the off-axis position exists, for which convincing experimental evidence has been provided.

In summary, in Part II of this paper both experimental verifications and potential applications have been presented indicating the consistency and practical value of the analysis presented in Part I.

ACKNOWLEDGMENTS

D. Li is supported by an University College Dublin–China Scholarship Council joint scholarship. We also acknowledge the support of the Science Foundation Ireland under the National Development Plan. D. P. Kelly is a Junior-Stiftungs professor of "Optik Design" and is supported by funding from Carl-Zeiss-Stiftung.

REFERENCES

1. D. Li, D. P. Kelly, and J. T. Sheridan, "Three-dimensional static speckle fields: part I. Theory and a numerical investigation," J. Opt. Soc. Am. A 28, 1896–1903 (2011).
2. L. Leushacke and M. Kirchner, "Three-dimensional correlation coefficient of speckle intensity for rectangular and circular apertures," J. Opt. Soc. Am. **7**, 827–832 (1990).
3. J. W. Goodman, *Speckle Phenomena in Optics: Theory and Applications*, 1st ed. (Roberts, 2007).
4. T. Yoshimura and S. Iwamoto, "Dynamic properties of three-dimensional speckles," J. Opt. Soc. Am. **10**, 324–328 (1993).
5. Q. B. Li and F. P. Chiang, "Three-dimensional dimension of laser speckle," Appl. Opt. **31**, 6287–6291 (1992).
6. A. Gatti, D. Magatti, and F. Ferri, "Three-dimensional coherence of light speckles: theory," Phys. Rev. **78**, 063806 (2008).
7. G. P. Weigelt and B. Stoffregen, "The longitudinal correlation of three-dimensional speckle intensity distribution," Optik **48**, 399–408 (1977).
8. C. E. Halford, W. L. Gamble, and N. George, "Experimental investigation of the longitudinal characteristics of laser speckle," Opt. Eng. **26**, 1263–1264 (1987).
9. J. E. Ward, D. P. Kelly, and J. T. Sheridan, "An alignment technique based on the speckle correlation properties of Fresnel transforming optical systems," Proc. SPIE **7068**, 70680L (2008).
10. J. E. Ward, "Optical metrology, speckle control, and the reduction of image degradation due to atmospheric turbulence," Ph.D. dissertation (University College Dublin, 2009).
11. T. Fricke-Begemann, "Three-dimensional deformation field measurement with digital speckle correlation," Appl. Opt. **42**, 6783–6796 (2003).
12. D. P. Kelly, B. M. Hennelly, and J. T. Sheridan, "Magnitude and direction of motion with speckle correlation and the optical fractional Fourier transform," Appl. Opt. **44**, 2720–2727 (2005).
13. D. P. Kelly, J. E. Ward, B. M. Hennelly, U. Gopinathan, F. T. O'Neill, and J. T. Sheridan, "Paraxial speckle-based metrology system with an aperture," J. Opt. Soc. Am. **23**, 2861–2870 (2006).
14. B. Bhaduri, C. Quan, C. J. Tay, and M. Sjödahl, "Simultaneous measurement of translation and tilt using digital speckle photography," Appl. Opt. **49**, 3573–3579 (2010).
15. Wolfram Research, http://reference.wolfram.com/mathematica/ref/Interpolation.html.